HHS Public Access

Author manuscript

J Biomed Mater Res B Appl Biomater. Author manuscript; available in PMC 2016 July 08.

Effects of Particle Size and Porosity on *In Vivo* Remodeling of Settable Allograft Bone/Polymer Composites

Edna M. Prieto[1,2,*], **Anne D. Talley**[1,2,*], **Nicholas R. Gould**[1], **Katarzyna J. Zienkiewicz**[1], **Susan J. Drapeau**[3], **Kerem N. Kalpakci**[3], and **Scott A. Guelcher**[1,2,4]

[1]Department of Chemical and Biomolecular Engineering, Vanderbilt University, Nashville, TN

[2]Center for Bone Biology, Vanderbilt University Medical Center, Nashville, TN

[3]Medtronic Spinal and Biologics, Memphis, TN

[4]Department of Biomedical Engineering, Vanderbilt University, Nashville, TN

Abstract

Established clinical approaches to treat bone voids include the implantation of autograft or allograft bone, ceramics, and other bone void fillers (BVFs). Composites prepared from lysine-derived polyurethanes and allograft bone can be injected as a reactive liquid and set to yield BVFs with mechanical strength comparable to trabecular bone. In this study, we investigated the effects of porosity, allograft particle size, and matrix mineralization on remodeling of injectable and settable allograft/polymer composites in a rabbit femoral condyle plug defect model. Both low viscosity (LV) and high viscosity (HV) grafts incorporating small (<105 μm) particles only partially healed at 12 weeks, and the addition of 10% demineralized bone matrix did not enhance healing. In contrast, composite grafts with large (105 – 500 μm) allograft particles healed at 12 weeks post-implantation, as evidenced by radial μCT and histomorphometric analysis. This study highlights particle size and surface connectivity as influential parameters regulating the remodeling of composite bone scaffolds.

Keywords

bone graft; polyurethane(s); composite/hard tissue; tissue engineering; animal model

Introduction

Established clinical approaches to treat bone voids include the implantation of autograft or allograft bone, ceramics, and other bone void fillers (BVF) [1]. While these materials offer a temporal solution to large bone loss, they do not fulfill all the targeted requirements for ideal bone grafts, including degradability, osteoconductivity, controlled degradation to non-toxic breakdown products, porosity, and mechanical strength comparable to that of the

Correspondence to: Scott A. Guelcher.

*Equally contributing authors

Conflict of Interest

S.A.G. is a consultant for Medtronic Spinal and Biologics, and the preclinical rabbit study was funded by Medtronic.

surrounding host trabecular bone [2–4]. Using minimally invasive surgical techniques, injectable and settable BVFs can be administered as a reactive liquid that subsequently cures to form a solid graft with bone-like mechanical properties [5]. Injectable calcium phosphate cements (CPCs) have proven to be superior to autograft for maintaining articular congruence of tibial plateau fractures due to their higher compressive strength [6].

Ceramic/polymer composites offer the potential advantage of improving the mechanical properties of brittle ceramics by combining them with weaker but ductile polymers [7]. While biodegradable polymers have tunable mechanical, degradation, and handling properties, their osteoconductivity is usually low. Ceramics provide bioactivity and osteoconductivity, although slow degradation rates and brittle mechanical properties can reduce their effectiveness, particularly for weight-bearing applications [8]. Composite bone scaffolds combining different ceramic phases and polymers have been reported to offer improved mechanical stability [9] and tissue interaction [2, 3] while providing injectability [10, 11], settability, and weight-bearing capabilities [12, 13].

Composites prepared from lysine-derived polyurethanes can be injected as a reactive liquid and set to yield BVFs with mechanical strength comparable to trabecular bone [14, 15]. When implanted in femoral plug bone defects in rats [14, 16], rabbits [12, 17], or sheep [11], they generate a minimal and transient inflammatory response, support cellular infiltration and new bone formation, and degrade to non-cytotoxic compounds. Both low- and high-viscosity allograft/poly(ester urethane) BVFs have been shown to remodel by creeping substitution [12, 15, 17], in which osteoclasts infiltrate the material along the surface of the mineralized particles and osteoblasts subsequently deposit new mineralized matrix. While these allograft/polymer BVFs remodel and support new bone formation, the effects of the allograft component on healing has not been extensively investigated.

In this study, we investigated the effects of allograft particle size, allograft particle loading, and allograft mineralization on remodeling and healing of allograft/poly(ester urethane) composite BVFs in a rabbit femoral condyle plug defect model. Two types of BVFs were investigated: (1) high-viscosity (HV) formulations incorporating 67 wt% allograft particles, and (2) low-viscosity (LV) formulations incorporating 46 wt% allograft. After injection, LV formulations expanded approximately two-fold in volume to yield BVFs with ~50% porosity, which consequently diluted the allograft content initially present in the reactive mixture. While HV grafts offer the advantage of bone-like strength [12], LV grafts were anticipated to support faster cellular infiltration and remodeling. The effects of particle size were also investigated. Considering that enhanced allograft resorption and new bone formation have been associated with small particles due to their greater specific surface area [18], we hypothesized that smaller allograft particles would increase healing. Finally, demineralized bone matrix was added at 9.6 wt% (the maximum amount that allowed for injectability) to some of the LV grafts to enhance their osteoinductivity. LV and HV formulations were injected into femoral plug defects in rabbits and remodeling evaluated at 6 and 12 weeks using micro-computed tomography, histology, and histomophometry.

Materials and Methods

Materials

Lysine-triisocyanate prepolymer (LTI-PEG, 21.7% NCO) was provided by Medtronic, Inc. (Memphis, TN). Glycerol, stannous octoate, and ε-caprolactone were purchased from Sigma-Aldrich (St. Louis, MO). Glycolide and DL-lactide were supplied by Polysciences (Warrington, PA). Rabbit allograft mineralized bone particles and demineralized bone matrix (DBM) were also received from Medtronic, Inc. Allograft particles and DBM were frozen and lyophilized before use to minimize water content. Triethylenediamine (TEDA) catalyst and dipropylene glycol (DPG) were purchased from Aldrich (St Louis, MO) and mixed to obtain a 10% (w/v) solution of TEDA in dry DPG.

Synthesis of polyester triol

Polyester triol was synthesized as previously described [19, 20]. Briefly, glycerol was mixed with ε-caprolactone, glycolide, and DL-lactide and stannous octoate catalyst under argon at 140 °C for 40 hrs. Afterwards, the polyester triol was cooled, washed with hexane, and dried under vacuum at 80 °C. The backbone of the polyester consisted of 70% ε-caprolactone, 20% glycolide, and 10% DL-lactide, produced at a molecular weight of 450 g mol^{-1}.

Synthesis of injectable and moldable composites

Table 1 summarizes the settable formulations included in this study, which are divided into low-viscosity (LV, 47 wt% allograft) and high-viscosity (HV, 67 wt% allograft) composites. All composites were prepared by loading a mixing cup with the appropriate amounts of polyester triol, LTI-PEG, catalyst, and allograft particles followed by hand mixing for 1 min. The index (ratio of isocyanate:hydroxyl equivalents x 100) for the LV and HV formulations was 115 and 130, respectively. LV composites contained 3400 ppm of TEDA catalyst, and HV composites were prepared with 5500 ppm TEDA. The effect of allograft particle size on the performance of the LV and HV composites was investigated by sieving the particles. Large (L) particles were first passed through a 500-μm sieve. Particles retained on the sieve were discarded, while those passing through the sieve were screened again through a 105-μm sieve. The resulting 105 – 500 μm fraction had a mean particle size of 180 +/− 70 μm. Small (S, <105 μm) particles were selected as those passing through the 105-μm sieve. In addition, a portion of the allograft component was replaced with DBM for some LV formulations (D) to evaluate its osteoinductive effect. Poor handling properties and lack of cohesiveness precluded the use of DBM in the HV composites. LV composites contained the maximum amount of allograft that allowed the material to be delivered by injection into the defect. The DBM content was chosen as the maximum amount that did not affect the cohesion of the LV composite (9.7 wt%). HV composites were formulated with high loading of allograft particles to provide a pathway for cells to infiltrate the composites through creeping substitution [17, 21].

Pore size and porosity

Thin sections of cured specimens were sputter-coated for 45 s using a Cressington Q108 sputter coater, which deposited gold at a 30mA current, and imaged using scanning electron

microscopy (Hitachi S-4200 SEM). Images (n=3 per formulation) were analyzed for pore size using ImageJ 1.47 image analysis software. Porosity of test specimens (n=3 per formulation) was determined gravimetrically by measuring height and diameter with calipers and weighing the samples to calculate density.

Rheological analysis: initial viscosity and working time

The initial flow characteristics of the composites were analyzed by removing the catalyst from the formulation (n=3). Non-setting samples were poured between 40-mm cross-hatched parallel plates, compressed to a gap of 1.5 mm, and subjected to a dynamic frequency sweep (0.1 to 100 rad sec^{-1}) at 25°C with controlled strain amplitude of 0.02%. A Cox-Merz transformation was applied to the dynamic data to obtain the steady state viscosity (η, Pa*s) as a function of shear rate (γ, s^{-1}). The data were fit to the Herschel-Bulkley model, which relates the viscosity and shear rate of solid-filled suspensions with high solids content [22], to estimate the yield stress (τ_Y, Pa) of the material:

$$\eta = \tau_Y \gamma^1 + K\gamma^{(n-1)} \quad (1)$$

where K is the consistency index of the composite (constant) and n is the power-law index of the suspending polymer. In this case, the suspending polymer corresponds to the non-reactive mixture of polyester triol and LTI-PEG prepolymer and has been shown to exhibit a Newtonian behavior (n=1) [12].

The curing profile of the composites was determined using a TA Instruments AR2000ex rheometer. Reactive composites were loaded between 25-mm diameter disposable plates and compressed to a gap of 1.5 mm. Measurements of storage (G′) and loss (G″) moduli were performed using an oscillatory time sweep method with a frequency of 1 Hz and amplitude of 1% strain. The working time of the formulations, defined as the time from the start of mixing until cure, was determined as the G′-G″ cross-over point.

Animal Study

Twenty-eight New Zealand White (NZW) rabbits were used in this study. All surgical and care procedures were carried out at IBEX Preclinical Research, Inc. (Logan, UT) under aseptic conditions per the approved IACUC protocol. The reactive components (LTI-PEG prepolymer, polyester triol, catalyst solution, and allograft) were gamma-irradiated using a dose of 25 kGY. Bilateral critical-size defects of 5 mm diameter by 6–8 mm in depth were drilled in the lateral femoral condyles of each rabbit. Metal wires were placed in the distal-most aspect of the defects to aid in location. Defects were filled with LV or HV formulations (n=4 defects per formulation) according to a randomized experimental design (different formulations were placed in contralateral defects). Control defects were left untreated (Empty). Femoral specimens were harvested after 6 and 12 weeks and placed in 10% neutral buffered formalin for fixation.

Micro-computed tomography (μCT) analysis

A μCT80 (SCANCO Medical, Basserdorf, Switzerland) was used to acquire images of the extracted femurs post implantation at 6 and 12 weeks. In addition, femurs from NZW rabbits

that were part of other experimental protocols that did not affect the skeleton (same age, sex, and similar weight to the rabbits used in this study) were scanned and analyzed as host bone controls. μCT scans were performed in formalin at 70 kVp energy, 114 μA source current, 250 projections per rotation, 400 ms integration time, and an isotropic voxel size of 36 μm. Axial images were reconstructed using manufacturer-provided software. Attenuation values were converted to tissue mineral density (TMD) through calibration with hydroxyapatite (HA) phantoms with densities between 0 and 780 mg HA cm^{-3} (calibration of the instrument was checked weekly). Using the cortical borders of the defect for alignment, the reconstructed image stack was re-oriented such that the depth of the defect was parallel to the z-axis. A radial analysis of morphometric parameters was conducted from the core of the implant to the interface with host bone. Three concentric annular volumes of interest with thickness of 1mm and a cylindrical core with diameter of 1mm all with approximate length of 7mm (from the outer cortical surface of the femur) were defined for each sample. The 3 inner regions covered the defect volume, while the outer region provided information about the interface with host bone. Ossified tissue was segmented from soft tissue using lower and upper thresholds of 140 mgHAcm^{-3} and 254 mgHAcm^{-3} respectively, as well as Gaussian noise filter settings of sigma 0.2 and support 2. Threshold conditions were chosen visually and kept constant for the analysis of all the samples. An upper threshold was included to avoid the selection of the metal wires as ossified tissue. Morphometric parameters within the annular regions were calculated, grouped by treatment and time point, and plotted versus the mean radial distance (R_m) from the core of the defect ($R_m=(R_o+R_i)/2$, where R_o and R_i correspond to the outer and inner radius of each region, respectively). Bone volume/total volume (BV/TV), trabecular number (Tb.N.), trabecular thickness (Tb.Th.), and trabecular separation (Tb.Sp.) within the regions of interest were computed using SCANCO's Medical microCT systems software.

Histology

After fixation in formalin, femur specimens were trimmed and embedded in methyl methacrylate. Thin sections were cut in a longitudinal plane through the approximate center of each defect. Care was taken to ensure that the orientation was as similar as possible between specimens. Sections of parallel planes were stained with Goldner's trichrome stain and Hematoxylin and Eosin (H&E) stain to evaluate the *in vivo* response of the different formulations. H&E sections were evaluated for inflammation and the presence of multi-nucleated osteoclast-like cells (OCL). Histological sections were imaged at either 70X or 140X for qualitative evaluation.

Histomorphometry

For quantitative analysis, Goldner's trichrome stained sections were imaged at 10X magnification with an Olympus camera (DP71) using an Olympus BX60 microscope. Residual allograft bone particles, newly formed bone, and residual polymer were quantified in an area of interest 1 mm high × 5 mm wide located in the center of the defect. To analyze the radial remodeling of the scaffolds in time, the rectangular area of interest was further subdivided into 3 concentric annular regions (each 0.83 mm thick) representing (1) the area of the defect in contact with the host bone, (2) the mid-region of the defect, and (3) the core of the defect. Mineralized tissue stained green, and to differentiate between the new bone

and the residual allograft, the allograft particles were identified as meeting the following two criteria: (1) acellular, and (2) angular shape. In the stained sections remaining polymer appeared white, newly deposited osteoid stained red/fucsia, cellular nuclei stained blue, and red blood cells stained orange/red. For histomorphometric analysis, Metamorph (Version 7.0.1) was utilized to color threshold each phase, quantify the number of pixels of each material and compare it to the total pixels in the area of interest. Similar to the μCT data, the content of new bone, residual mineralized allograft bone, and residual polymer was plotted as a function of the mean radial distance from the core of the defect (R_m). Goldner's trichrome stain did not reveal DBM particles, so these were not included in the histomorphometric analysis. Initial content of allograft bone and polymer in each formulation was determined from histological sections of scaffolds prepared in the laboratory and processed as described in the previous section.

Considering previous studies pointing to surface connectivity as a critical parameter controlling healing [12], Euler numbers (Eu) were calculated for each concentric annular region of the histological sections to determine the surface connectivity of the grafts [23]. The Euler number quantifies the surface connectivity of an image:

$$Eu = C - H \quad (2)$$

where *C* corresponds to the number of continuous objects and *H* to the number of holes [24]. Thus, $Eu = 1$ represents an image without holes, $Eu \gg 1$ an image with low surface connectivity, and $Eu \ll 1$ a highly connected image. Residual allograft particles, new bone, and residual polymer were selected from histomorphometry images as connected objects (*C*), and pores and voids were identified as holes (*H*) using GIMP 2.6.11. The thresholded images were converted to binary files (Image J 1.47p) and then used to calculate *Eu* in MATLAB R2011a. The percentage of the defect healed in each region of interest (ROI) was calculated as:

$$\%\,\text{healed} = \frac{\text{area}\,\%\,\text{new bone in ROI}}{\text{area}\,\%\,\text{bone in untreated control}} \quad (3)$$

where the untreated control exhibited 38% bone. The percentage healed was plotted versus *Eu* for all regions.

Statistical analysis

A one-way analysis of variance (ANOVA) was performed to compare the rheological properties, pore size, and porosity of different treatment groups. Three-way ANOVAs were run in JMP 11.1.1 to determine if statistical differences existed between time, radial area, and composition for the *μCT* morphometric parameters and histomorphometry data. Individual samples were compared by running a Tukey honestly significant difference (HSD) test. Statistical significance was considered for $p < 0.05$.

Results

Composite characterization

Rheological testing of the non-reactive and reactive formulations provided information about their handling properties. HV composites had the lowest working times (5 – 6 min), and addition of DBM delayed the setting of LV formulations (Table 1). Figure 1 shows representative curves for the initial viscosity of HV and LV composites as a function of shear rate. LV formulations with small particles exhibited Newtonian behavior at shear rates below ~3 s^{-1} (initial plateau), followed by power-law behavior at larger shear rates. The Herschel-Bulkley model [22] was used to calculate the yield stress (Table 1) for the LV-LD and HV groups (the LV-S and LV-SD groups showed minimal evidence of yield stress). The LV-LD, HV-L, and HV-S groups exhibited power law behavior even at low shear rates. The addition of DBM increased the initial viscosity (evaluated at 5 s^{-1} [25]).

As expected, HV composites had lower porosity than LV (Table 1). Representative images (Figure 2) suggest that porosity of HV formulations was associated with voids present between allograft particles, or between allograft particles and polymer (the size of the pores was not measured due to the difficulty of identifying the pores). In contrast, gas foaming due to the reaction of the NCO-terminated prepolymer with water was the main source of porosity for LV composites. Particle size also influenced porosity and pore size in LV composites with DBM. Comparison of LV-LD to LV-SD shows a 3-fold increase in pore size (Figure 2) and a more modest but significant 30% increase in porosity (Table 1) for formulations with large compared to small allograft particles (Figure 2).

μCT analysis

Representative μCT images of all the treatment groups after 6 and 12 weeks in the rabbits are presented in Figure 3A. Empty defects healed <10% and only showed new bone near the femoral cortex. Large residual allograft particles could be identified in the images, particularly at 6 weeks (irregularly shaped radiolucent particles). Visual changes between the 6 and 12 week images of the composites suggest ongoing remodeling.

Allograft/polymer composites remodel by creeping substitution as cells infiltrate the scaffold from the host bone-scaffold interface to the core [17]. Thus, morphometric parameters evaluated by μCT were plotted as a function of the mean radial distance from the core of the defect (Figure 3B). The BV/TV data, which include both new bone and residual allograft, showed progressive healing in both space and time. At 6 weeks, both LV and HV composites exhibited substantially higher BV/TV (~50%) compared to host bone (29.7±1.3%), suggesting densification of the interface in response to grafting. For HV composites, BV/TV remained relatively constant from the host bone interface to the inner core and was significantly higher than LV grafts at the two innermost regions. In contrast, BV/TV monotonically decreased from the interface to the core for LV composites (differences not significant). In the inner core region, BV/TV = 6 – 17%, which is in the range of initial allograft concentration, suggesting that the cells have not yet reached the interior of the composite at 6 weeks. By 12 weeks, BV/TV for all groups approached host bone values and was less dependent on radial position than at 12 weeks, with no significant

differences between HV and LV groups at any radial position. While the shape of the radial BV/TV profiles changed from 6 to 12 weeks for all groups, only HV-L (outer two regions), LV-LD (interfacial region), and LV-SD (interfacial region) showed significant differences in BV/TV versus time.

Analysis of key morphometric parameters provides additional information about the remodeling mechanism of the composites (Figure 3B). Tb.N. (average number of trabeculae per unit length [26]) is initially a measure of the volume fraction of allograft bone. Thus, HV formulations initially had higher Tb.N. than LV. The radial distribution of Tb.N. at 6 weeks showed opposite trends between HV and LV. HV grafts exhibited a radial decrease in Tb.N., suggesting either allograft resorption or increased surface connectivity of the residual allograft, from the core to the interface. Tb.N. for HV-S was significantly higher than HV-L in the inner two regions due to the larger numbers of allograft particles present. In contrast, Tb.N. of LV formulations increased radially, suggesting the creation of new trabeculae near the host bone interface, with Tb.N. significantly lower than that of HV groups at the inner two radial regions. At 12 weeks, the values of Tb.N. approached those of host bone for all groups and regions. Differences in Tb.Th. (mean thickness of trabeculae [26]) between grafts with large and small particles at 6 weeks in the core region are likely due to differences in allograft particle size. Tb.Th. increased for all the groups from the core to the interface at 6 and 12 weeks, suggesting new bone deposition as cells infiltrate the materials, but the differences were not significant. The parameter Tb.Sp. (mean distance between trabeculae [26]) in the inner core at 6 weeks reflects differences in initial porosity between HV (Tb.Sp.<0.02 mm) and LV (Tb.Sp.>0.05 mm) groups. Thus, at 6 weeks Tb.Sp. increased for HV grafts and decreased for LV grafts with radial distance from the core (HV groups were significantly lower than LV-SD at the two innermost regions). At 12 weeks, Tb.Sp. was relatively independent of radial position and slightly exceeded that of host bone.

Histology

Representative low-magnification images of histological sections at 6 and 12 weeks (Figure 4) reveal that empty defects did not heal and were largely filled with fatty bone marrow surrounded by a shell of bone. In contrast, images of treated defects suggest that large allograft particles promoted more balanced remodeling compared to small particles. Histological sections stained for H&E revealed that none of the treatment groups generated acute inflammation at 6 or 12 weeks (data not shown). Small numbers of inflammatory cells were present at 6 weeks and decreased with time.

High-magnification images of histological sections (Figure 5) reveal active remodeling of the grafts, as evidenced by the presence of bone lining cells. At 6 weeks, new bone formation was ongoing predominantly at the periphery of treated defects, while the central area remained largely acellular. Osteoid (OD) lined with active osteoblasts was present both at 6 and 12 weeks. New bone was deposited appositionally mostly by intramembranous ossification, except at the periphery of the defects where endochondral ossification was present (in particular at 6 weeks). New bone deposited at early time points exhibited a woven bone (WB) structure for all treatment groups. Many specimens also revealed evidence of more organized lamellar bone (LB), particularly at 12 weeks. After 12 weeks,

residual allograft particles (light blue, A) were incorporated with new bone (dark blue), which was more extensive in scaffolds with large particles. Many islands of new bone were visible in small particle composites, whereas a more continuous new bone phase was present in large particle composites. Multi-nucleated osteoclast-like cells (OCL) were associated with residual allograft (A) particles and contained intracellular material (arrows in Figure 5, LV-SD at 6 weeks).

Histomorphometry

Histomorphometry provided quantitative measurements of new bone formation, residual allograft, and residual polymer in each region for each treatment group (Figure 6). Total mineralized tissue (new bone and allograft, % NB+A) showed similar trends to BV/TV measured by μCT (Figure 3B). At 6 weeks, all groups showed greater new bone formation near the host bone interface and less new bone formation near the core, suggesting limited cellular infiltration of the core. At 12 weeks, all of the treatment groups achieved a similar amount of new bone near the host bone interface. Grafts with large particles (LV-LD and HV-L) showed more new bone in the core region compared to those with small particles (LV-SD, LV-S, and HV-S), but the differences were not significant. Due to their higher initial allograft content, at 6 weeks HV grafts showed 10–15% more residual allograft in the inner two regions and 10% less polymer in the core compared to LV. For all groups, residual allograft and polymer were lower near the interface than the core, which is consistent with the notion that at 6 weeks the inner regions are less infiltrated with cells. At 12 weeks, <5% residual allograft and polymer remained in all groups except for HV-S.

The percentage of the defect healed was plotted versus Euler number (*Eu*, eq (2)) to assess the effects of surface continuity on healing (Figure 7A). Healing generally increased with increasing Euler number. However, in the inner core of the small particle groups (LV-SD, LV-S, and HV-S) at 12 weeks, healing was <50% at $Eu > 20$ (dashed line box in Figure 7A). Representative images of healing sections with $Eu < 5$ (Figure 7B) show a more inter-connected surface, while images of non-healing sections ($Eu > 20$, Figure 7C) show isolated islands of new bone, polymer, and allograft that are too far apart to be bridged by new bone.

Discussion

As a biocompatible and osteoconductive alternative for autograft, surgeons have been using allograft bone for more than 20 years [27, 28]. Allograft bone particles can be mixed with flowable polymers to facilitate injectability. However, injectable allograft bone composites typically have weak mechanical properties and are not compression-resistant. We have previously described injectable and settable allograft composites prepared from lysine-derived polyisocyanates and polyester triols [10, 12, 14, 15]. These materials promote cellular infiltration, allograft resorption, and new bone formation when implanted in femoral condyle plug defects. However, allograft/poly(esterurethane) composites did not heal at late time points due to a mismatch between the rates of new bone formation and polymer degradation [12]. The aim of the present study was to investigate the effects of allograft particle size, loading and mineralization on healing of femoral plug defects in rabbits grafted with injectable, settable allograft/polymer composites.

As anticipated, HV grafts exhibited higher initial viscosity than LV grafts (Figure 1) due to their higher solids content. For LV grafts, viscosity increased with increasing particle size (0.017 kPa*s for LV-S versus 0.17 kPa*s [15] for LV-L) and DBM content. Addition of DBM increased the initial viscosity from 0.017 to 0.07 kPa*s for LV-S grafts and from 0.17 [15] to 30.2 kPa*s for LV-L grafts, which is consistent with studies reporting an increase in the resistance of polymers to flow as a consequence of clustering of incompatible (fibrous versus granular) particles [29]. The effect of DBM was most dramatic for LV-L composites, which showed a 175-fold increase in initial viscosity at 5 s^{-1} as well as more pronounced shear-thinning behavior. This observation suggests that the effects of mixing fibrous and granular particles on viscosity were most significant for large particles. An additional effect of small particles in LV grafts was the unexpected significant reduction in pore size (Figure 2). It is conjectured that the increased number of small versus large allograft particles generated a more tortuous path for the CO_2 gas to escape, resulting in more pores that are smaller in size. Interestingly, the effect of particle size on viscosity was reversed for HV grafts, which showed decreasing viscosity with increasing particle size.

Contrary to our expectations, the addition of DBM to LV formulations hindered remodeling of the rabbit femoral plug defects. DBM has been reported to be osteoinductive and to stimulate defect healing in dogs [30, 31], rabbits [32], and humans [33]. However, at concentrations used in the present study (<10 wt%), which is the maximum value that supported injectability, it showed no evidence of osteoinductivity.

Considering a previous study speculating that the enhanced new bone formation associated with small particles is due to their greater specific surface area [18], we hypothesized that smaller allograft particles would improve healing. However, LV and HV grafts incorporating allograft particles <105 μm supported ~50% less new bone formation in the inner core than those with allograft particles in the size range of 100 – 500 μm at 12 weeks (Figure 6). In a previous study combining allograft bone particles with autogenous bone marrow, allograft particles ranging in size from 100 – 300 μm promoted significantly more new bone formation than larger particles (1000 – 2000 μm) when implanted in the femurs of Rhesus monkeys for 8 weeks [34]. A study in rabbit calvarial defects reported a greater amount of osteoid tissue and instead of particles with larger size (up to 1000 μm) [18]. Another study investigating the effect of particle size on the osseointegration of silicate-substituted calcium phosphates (Si-CaP) reported enhanced performance of particles with size in the range of 250–500 μm (36.5 +/− 2.3 area% new bone), while smaller particles (90–125 μm) promoted a less favorable healing outcome (30.4 +/− 3.5 area% new bone) [35]. Similarly, our results show 22 – 30 area% new bone in the inner core of LV and HV grafts incorporating 105–500 μm allograft particles after 12 weeks, compared to 10 – 16 area % new bone for grafts with small particles > 105 μm.

Interconnected porosity has long been considered a fundamental requirement for the success of bone scaffolds [4, 7]. However, in this study no significant differences in new bone formation were observed between high (35 – 45%) porosity LV and low (8 – 16%) porosity HV groups at 6 or 12 weeks. The radial analyses of morphometric parameters (Figures 4 and 6) suggest that cells infiltrate the grafts by resorption of both the allograft and polymer phases, which is consistent with previous studies reporting that allograft/polymer composites

remodel from the host bone interface to the interior of the graft by creeping substitution [12, 36]. The Euler number analysis (Figure 7) reveals two potential healing outcomes. In the inner core of the small particle groups (LV-SD, LV-S, and HV-S), healing was < 50% at *Eu* > 20. This observation suggests that the inner core region of grafts with < 105 μm particles are on a path to resorption, presumably due to the slower rate of new bone formation observed for smaller particles. In contrast, despite their differences in allograft loading and porosity, LV and HV grafts with 105 – 500 μm particles showed 50 – 100% healing as *Eu* increased to ~1, which is in the range reported for trabecular bone ($-1 < Eu < 1$ [23]). While this observation suggests that the grafts with large particles are progressing toward healing, the histomorphometric data in Figure 6 show that the polymer has completely degraded in all regions at 12 weeks. Consequently, premature degradation of the polymer in larger defects that require more time to heal may adversely affect remodeling. Further testing in large animal models is required to validate that injectable and settable allograft/polymer composites heal in larger defects at later time points.

Conclusions

In this study, we investigated the effects of allograft loading, particle size, and mineralization on remodeling of injectable and settable allograft/polymer composites in a rabbit femoral condyle plug defect model. Both low viscosity (LV) and high viscosity (HV) grafts incorporating small (<105 μm) particles only partially healed at 12 weeks, and the addition of 10% demineralized bone matrix did not enhance healing. In contrast, composite grafts with large (105 – 500 μm) allograft particles healed at 12 weeks post-implantation, as evidenced by radial μCT and histomorphometric analysis. This study highlights particle size and surface connectivity of the graft as influential parameters regulating the remodeling of composite bone scaffolds.

Acknowledgments

This material is based in part upon work supported by the National Science Foundation under Grant Number 0847711 (CAREER award to S.A.G.). Any opinions, findings, and conclusions or recommendations expressed in this material are those of the author(s) and do not necessarily reflect the views of the National Science Foundation. This work was supported by the Army, Navy, NIH, Air Force, VA and Health Affairs to support the AFIRM II effort, under Award No. W81XWH-14-2-0004. The U.S. Army Medical Research Acquisition Activity, 820 Chandler Street, Fort Detrick MD 21702-5014 is the awarding and administering acquisition office. Opinions, interpretations, conclusions and recommendations are those of the author and are not necessarily endorsed by the Department of Defense. The preclinical rabbit study was funded by Medtronic Spinal and Biologics. Anne Talley acknowledges support from the Department of Education for a Graduate Assistance in Areas of National Need Fellowship under grant number P200A090323. Instrumentation for μCT analysis was purchased with funds from NIH grant S10RR027631.

References

1. Woodruff MA, et al. Bone tissue engineering: from bench to bedside. Materials Today. 2012; 15(10):430–435.
2. Rezwan K, et al. Biodegradable and bioactive porous polymer/inorganic composite scaffolds for bone tissue engineering. Biomaterials. 2006; 27(18):3413–3431. [PubMed: 16504284]
3. Scaglione S, et al. A composite material model for improved bone formation. Journal of Tissue Engineering and Regenerative Medicine. 2010; 4(7):505–513. [PubMed: 20213628]
4. Bose S, Roy M, Bandyopadhyay A. Recent advances in bone tissue engineering scaffolds. Trends in Biotechnology. 2012; 30(10):546–554. [PubMed: 22939815]

5. Hak DJ. The use of osteoconductive bone graft substitutes in orthopaedic trauma. Journal of the American Academy of Orthopaedic Surgeons. 2007; 15(9):525–536. [PubMed: 17761609]
6. Russell TA, Leighton RK. Comparison of autogenous bone graft and endothermic calcium phosphate cement for defect augmentation in tibial plateau fractures. A multicenter, prospective, randomized study. J Bone Joint Surg Am. 2008; 90(10):2057–61. [PubMed: 18829901]
7. Wagoner Johnson AJ, Herschler BA. A review of the mechanical behavior of CaP and CaP/polymer composites for applications in bone replacement and repair. Acta Biomater. 2011; 7(1):16–30. [PubMed: 20655397]
8. Bohner M, Galea L, Doebelin N. Calcium phosphate bone graft substitutes: Failures and hopes. Journal of the European Ceramic Society. 2012; 32(11):2663–2671.
9. Jones JR. Review of bioactive glass: from Hench to hybrids. Acta Biomater. 2013; 9(1):4457–86. [PubMed: 22922331]
10. Page JM, et al. Biocompatibility and chemical reaction kinetics of injectable, settable polyurethane/allograft bone biocomposites. Acta Biomaterialia. 2012; 8(12):4405–16. [PubMed: 22871639]
11. Adhikari R, et al. Biodegradable injectable polyurethanes: Synthesis and evaluation for orthopaedic applications. Biomaterials. 2008; 29(28):3762–3770. [PubMed: 18632149]
12. Dumas JE, et al. Balancing the Rates of New Bone Formation and Polymer Degradation Enhances Healing of Weight-Bearing Allograft/Polyurethane Composites in Rabbit Femoral Defects. Tissue Eng Part A. 2013 Not available - ahead of print.
13. Kruger R, Groll J. Fiber reinforced calcium phosphate cements -- on the way to degradable load bearing bone substitutes? Biomaterials. 2012; 33(25):5887–900. [PubMed: 22632767]
14. Dumas JE, et al. Synthesis and Characterization of an Injectable Allograft Bone/Polymer Composite Bone Void Filler with Tunable Mechanical Properties. Tissue Engineering Part A. 2010; 16(8):2505–2518. [PubMed: 20218874]
15. Dumas JE, et al. Injectable reactive biocomposites for bone healing in critical-size rabbit calvarial defects. Biomedical Materials. 2012; 7(2):024112. [PubMed: 22456057]
16. Yoshii T, et al. Synthesis, characterization of calcium phosphates/polyurethane composites for weight-bearing implants. Journal of Biomedical Materials Research Part B-Applied Biomaterials. 2012; 100B(1):32–40.
17. Dumas JE, et al. Synthesis, characterization, and remodeling of weight-bearing allograft bone/polyurethane composites in the rabbit. Acta Biomaterialia. 2010; 6(7):2394–2406. [PubMed: 20109586]
18. Klüppel LE, et al. Bone Repair is Influenced by Different Particle Sizes of Anorganic Bovine Bone Matrix: A Histologic and Radiographic Study In Vivo. Journal of Craniofacial Surgery. 2013; 24(4):1074–1077.10.1097/SCS.0b013e318286a0a3 [PubMed: 23851743]
19. Guelcher S, et al. Synthesis, in vitro degradation, and mechanical properties of two-component poly (ester urethane) urea scaffolds: effects of water and polyol composition. Tissue engineering. 2007; 13(9):2321–2333. [PubMed: 17658992]
20. Guelcher SA, et al. Synthesis and in vitro biocompatibility of injectable polyurethane foam scaffolds. Tissue engineering. 2006; 12(5):1247–1259. [PubMed: 16771638]
21. Eagan MJ, McAllister DR. Biology of Allograft Incorporation. Clinics in Sports Medicine. 2009; 28(2):203–214. [PubMed: 19306730]
22. Poslinski AJ, et al. Rheological Behavior of Filled Polymeric Systems I. Yield Stress and Shear-Thinning Effects. Journal of Rheology. 1988; 32(7):703–735.
23. Portero-Muzy NR, et al. Euler strut. cavity, a New Histomorphometric Parameter of Connectivity Reflects Bone Strength and Speed of Sound in Trabecular Bone from Human Os Calcis. Calcified tissue international. 2007; 81(2):92–98. [PubMed: 17639366]
24. Pratt, W. Digital imaging processing. Canada: John Wiley & Sons; 2001.
25. Baroud G, Cayer E, Bohner M. Rheological characterization of concentrated aqueous beta-tricalcium phosphate suspensions: the effect of liquid-to-powder ratio, milling time, and additives. Acta Biomaterialia. 2005; 1(3):357–63. [PubMed: 16701814]

26. Bouxsein ML, et al. Guidelines for assessment of bone microstructure in rodents using micro–computed tomography. Journal of Bone and Mineral Research. 2010; 25(7):1468–1486. [PubMed: 20533309]
27. Ferreira CEA, et al. A Clinical Study of 406 Sinus Augmentations With 100% Anorganic Bovine Bone. Journal of Periodontology. 2009; 80(12):1920–1927. [PubMed: 19961375]
28. Pieri F, et al. Alveolar Ridge Augmentation With Titanium Mesh and a Combination of Autogenous Bone and Anorganic Bovine Bone: A 2-Year Prospective Study. Journal of Periodontology. 2008; 79(11):2093–2103. [PubMed: 18980518]
29. Li JQ, Salovey R. Model filled polymers: The effect of particle size on the rheology of filled poly(methyl methacrylate) composites. Polymer Engineering & Science. 2004; 44 (3):452–462.
30. Tiedeman J, et al. Treatment of nonunion by percutaneous injection of bone marrow and demineralized bone matrix. An experimental study in dogs. Clin Orthop Relat Res. 1991; 268:294–302. [PubMed: 2060222]
31. Frenkel S, et al. Demineralized bone matrix. Enhancement of spinal fusion. Spine (Phila Pa 1976). 1993; 18(12):1634–9. [PubMed: 8235843]
32. Damien C, et al. Effect of demineralized bone matrix on bone growth within a porous HA material: a histologic and histometric study. J Biomater Appl. 1995; 9(3):275–88. [PubMed: 9309501]
33. Simion M, et al. Qualitative and quantitative comparative study on different filling materials used in bone tissue regeneration: a controlled clinical study. Int J Periodontics Restorative Dent. 1994; 14(3):198–215. [PubMed: 7995691]
34. Shapoff CA, et al. The Effect of Particle Size on the Osteogenic Activity of Composite Grafts of Allogeneic Freeze-Dried Bone and Autogenous Marrow*†. Journal of Periodontology. 1980; 51(11):625–630. [PubMed: 7007609]
35. Coathup MJ, et al. The effect of particle size on the osteointegration of injectable silicate-substituted calcium phosphate bone substitute materials. Journal of Biomedical Materials Research Part B: Applied Biomaterials. 2013; 101B(6):902–910.
36. Oest ME, et al. Quantitative assessment of scaffold and growth factor-mediated repair of critically sized bone defects. Journal of Orthopaedic Research. 2007; 25(7):941–950. [PubMed: 17415756]

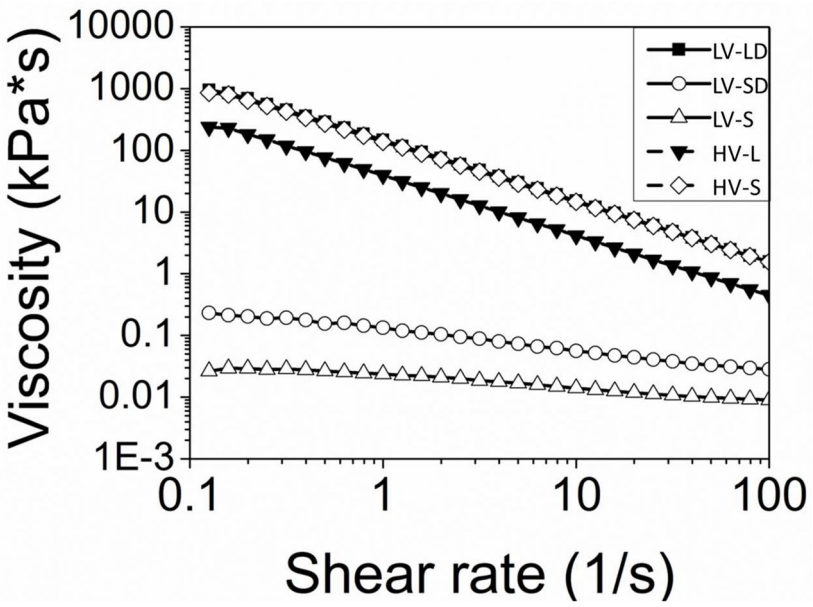

Figure 1. Initial viscosity of allograft/polymer composites

Non-reactive formulations were poured between 40-mm cross-hatched parallel plates, compressed to a gap of 1.5 mm, and subjected to a dynamic frequency sweep (0.1 to 100 rad sec^{-1}) at 25°C with controlled strain amplitude of 0.02% (n=3). Dynamic data was transformed steady state viscosity (η, Pa*s) as a function of shear rate (γ, s^{-1}) using a Cox-Merz transformation (geometric figures). Data were fit to the Herschel-Bulkley model (lines) to determine yield stress in the case of the LV-LD, HV-S, and HV-L formulations.

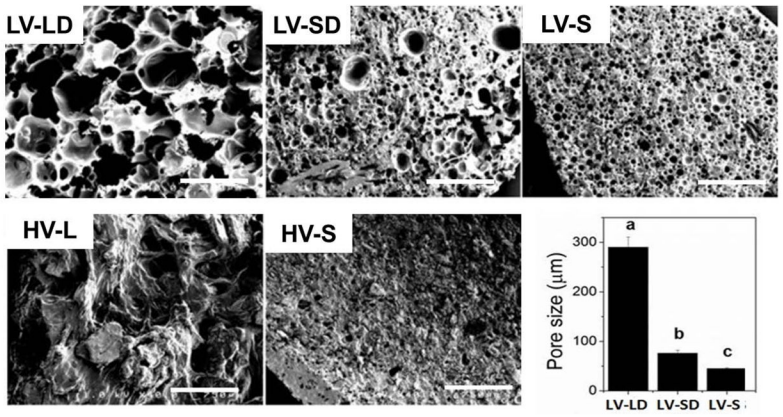

Figure 2. Scanning electron microscopy images and porosity of allograft/polymer composites

SEM images reveal pores present in LV grafts, while HV grafts show lower porosities. Scale bars represent 750 μm. The pore size measured from SEM images are shown in the bar chart for LV grafts. Statistically significant differences between groups ($p < 0.05$) are indicated by different letters.

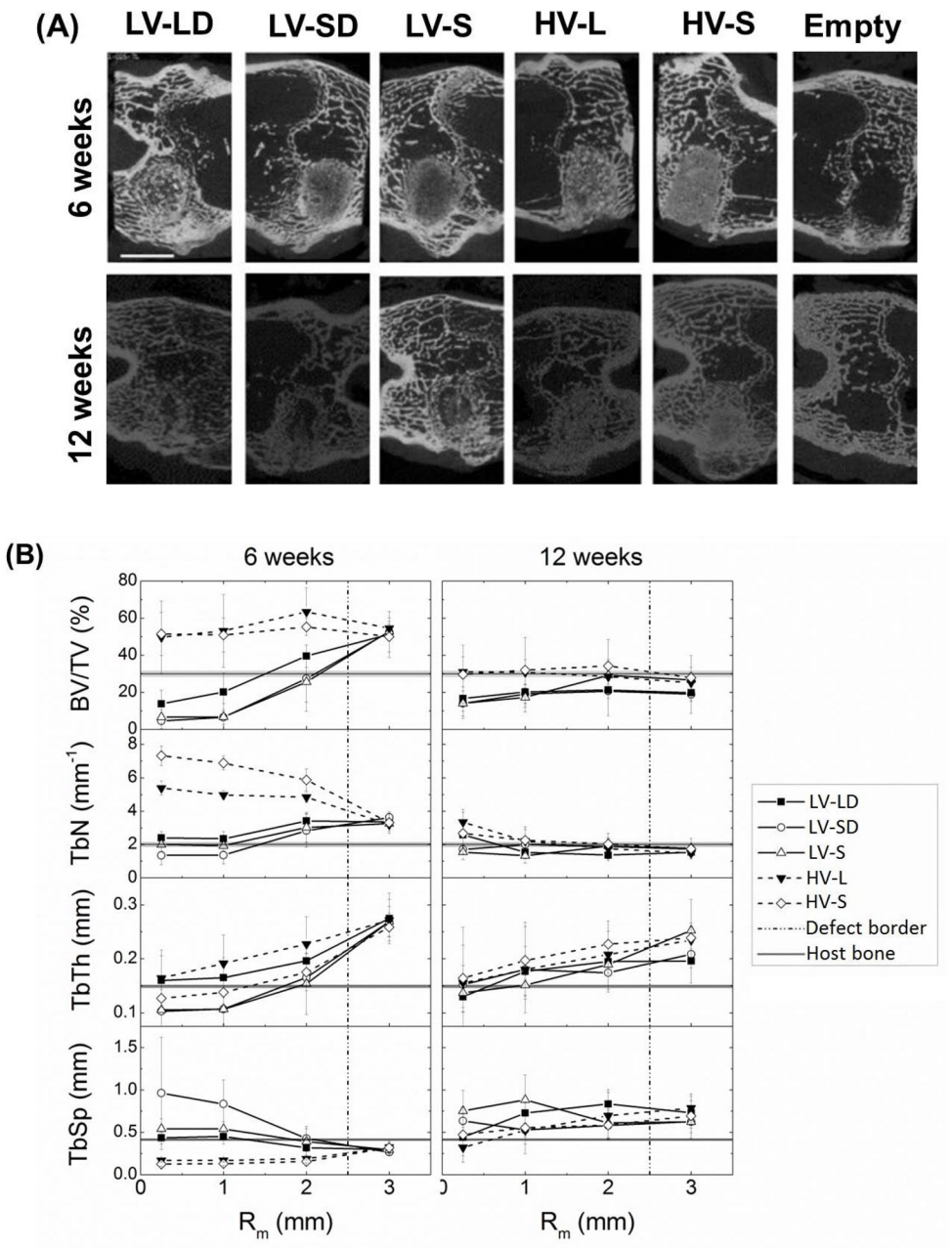

Figure 3. µCT analysis of mineralized tissue in allograft/polymer composites

(A) Representative µCT images at 6 and 12 weeks. Scale bar represents 5 mm. **(B)** The morphometric parameters BV/TV, Tb.N., Tb.Th., and Tb.Sp. were each measured as a function of radial distance from the center line of the defect at 6 and 12 weeks and compared to host bone values measured separately.

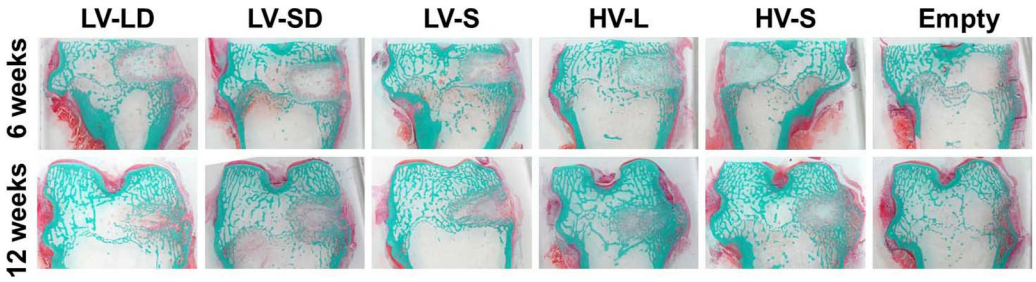

Figure 4. Low-magnification images of histological sections of allograft/polymer composites at 6 and 12 weeks

Sections were stained with Goldner's trichrome stain (original 1X magnification).

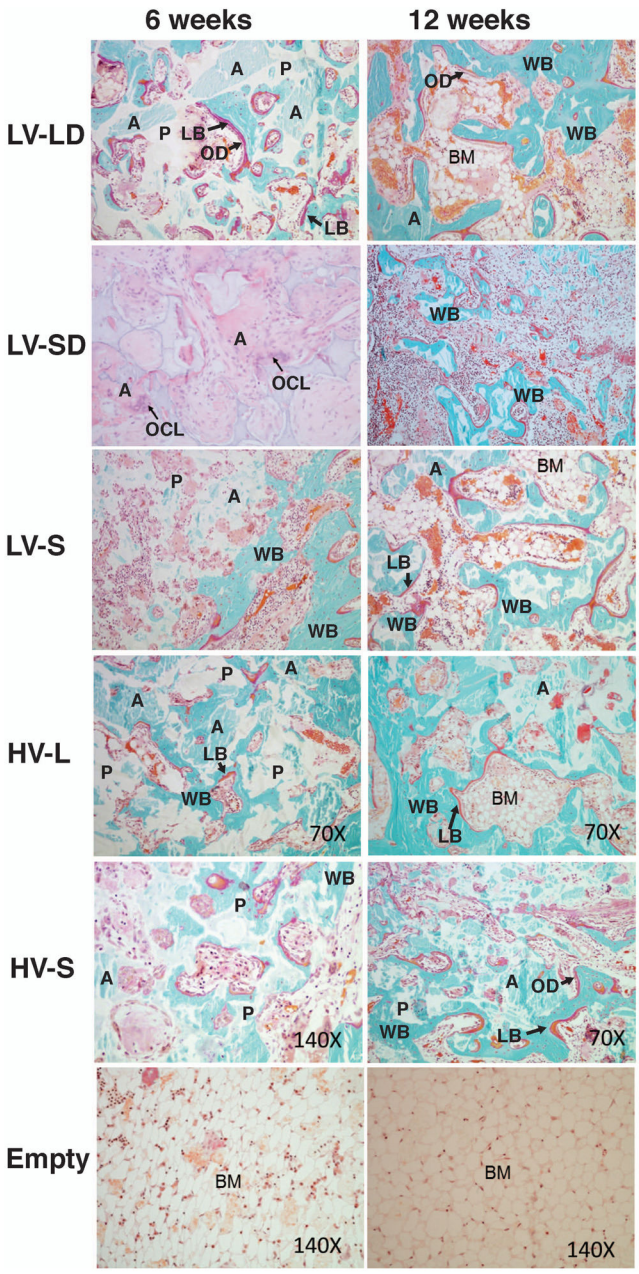

Figure 5. High-magnification images of histological sections of defects treated with injectable allograft/polymer composites

All of the images show sections stained with Goldner's trichrome except for LV-SD at 6 weeks, which is stained with H&E. Original magnification 70X. With Goldner's trichrome stain: *white*- residual polymer (P); *light blue particles with angled shapes*- residual allograft particles (A); *blue with cells inside*- new mineralized bone with osteocytes with a woven structure (WB); *red*- an organized lamellar bone structure (LB); *red bone lining cells*- osteoid (OD); and bone marrow (BM). Arrows in the LV-SD 6 weeks section point to multi-nucleated osteoclast-like cells (OCLs).

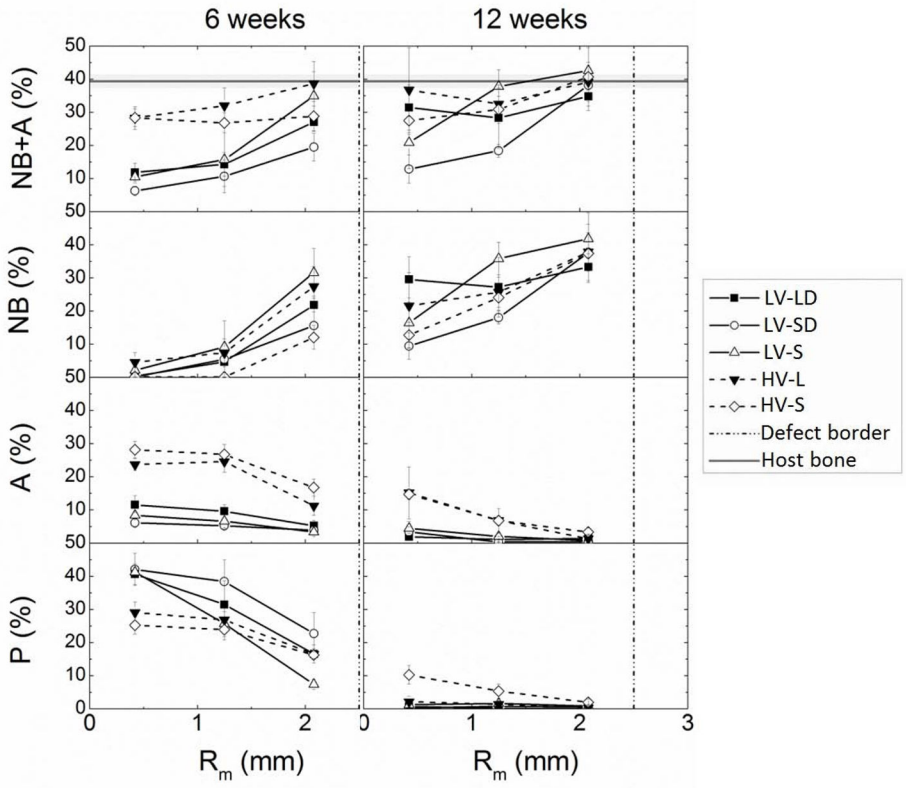

Figure 6. Histomorphometric analysis of new bone formation of allograft/polymer composites at 6 and 12 weeks

Total mineral content (NB+A, including new bone and residual allograft), new bone (NB), residual allograft (A), and residual polymer (P) data are plotted as a function of radial distance from the center line of the defect at 6 and 12 week.

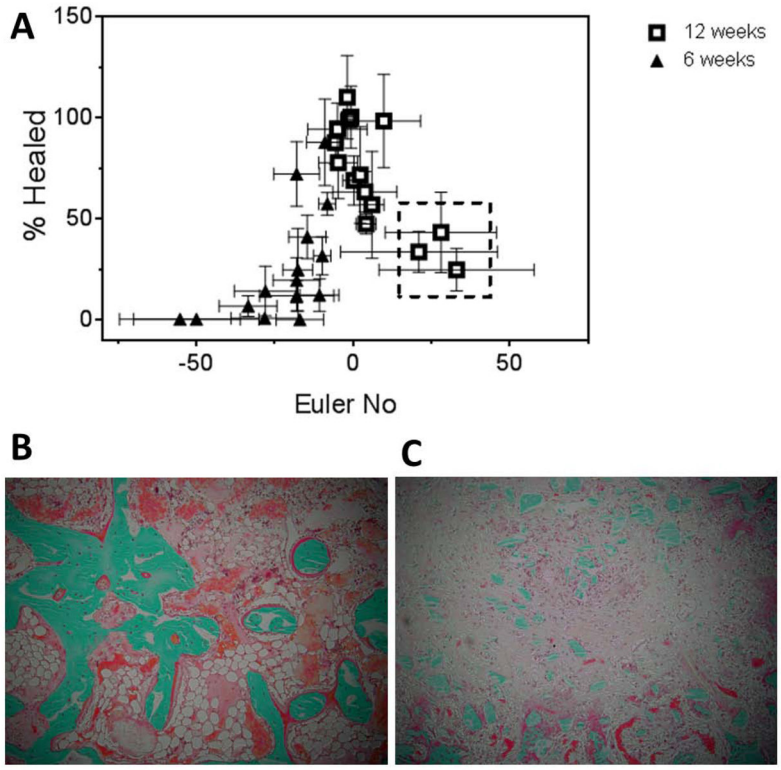

Figure 7. Assessment of healing progression by Euler number number analysis

(A) Plot of percent healed versus Eu for all samples. Grafts that supported <50% healing at Eu > 20 showed large resorption gaps due to the lack of an interconnected surface on which bone could grow. (B–C) High-magnification images of histological sections of grafts with (B) advanced healing and interconnected surface (Eu < 0), LV-LD sample at 12 weeks, and (C) poor healing and a non-interconnected surface (Eu > 20), LV-SD sample at 12 weeks.

Table 1

Composition and physical properties of PUR/allograft composites.

Treatment group	Category	Allograft (wt%)	DBM (wt%)	Particle size (μm)	Working time (min)	Viscosity at $5s^{-1}$ (kPa*s)	Yield stress (kPa)	Gravimetric porosity (%)
Empty	Control	N/A	N/A	N/A	N/A	N/A	N/A	N/A
LV-LD	Injectable	37.4	9.6	105–500	9.3±0.1[a]	30.2±4.5[a]	129±12[a]	45.0±1.4
LV-SD	Injectable	37.4	9.6	<105	9.5±0.3[a]	0.073	N/A	35.0±1.7[a]
LV-S	Injectable	47	0	<105	8.7±0.1	0.017	N/A	38.3±0.5[a]
HV-L	Moldable	67	0	105–500	5.3±0.1	8.1±3.6	34±17	16.3±2.3
HV-S	Moldable	67	0	<105	5.9±0.1	28.7±0.01[a]	119±4[a]	7.7±0.7

LV: Low Viscosity; HV: High Viscosity; L: large allograft particles; S: small allograft particles; D: contains DBM

[a]Groups with the same letter are statistically the same (p>0.05)

Reported error corresponds to the standard error of the mean